

Experimental and numerical analysis of uni-axial buckling of single-phase functionally graded porous polymeric sandwich plates

Emad K. Njim^{1*}, Mohammad H. Almamuri², Sadeq H. Bakhy³, Zainab S. Idan⁴, Muhannad Al-Waily⁵, Mohsen J. Jweeg⁶ and L. Hadji⁷

¹Ministry of Industry and Minerals, State Company for Rubber and Tires Industries, Iraq

²Biomaterials Engineering Department, Faculty of Engineering, University of Al-Mustaqbal, IRAQ.

³University of Technology, Mechanical Engineering Department, Baghdad, Iraq

⁴Department of Computer Technical Engineering, college of Technical Engineering, university of Akafeel, Al-Najaf, Iraq,

⁵Department of Mechanical Engineering, Faculty of Engineering, University of Kufa, Iraq

⁶Al-Farahidi University, College of Technical Engineering, Iraq.

⁷Department of Mechanical Engineering, University of Tiaret, Tiaret, Algeria

Abstract. The porosity gradient functionally graded material (PFGM) is one of the most popular types of FGM, in which the porosity in the material is made to change in the specified direction. This study looks into the buckling problems of rectangular sandwich plates made of single-phase porous functionally graded materials (PFGMs), commonly used in aircraft structures and biomedical applications. A compression test was performed on the 3D-printed polymeric FG specimens bonded with two thin solid face sheets on the upper and lower surfaces. The critical stress of well-designed and fabricated 3D printed FGM plate samples with various metal core types is determined using a PC installed on universal testing equipment (UTM). The effect of different essential parameters (such as porous ratio, gradient exponent, and aspect ratio) on buckling load and total deformation were explored. The finite element method (FEM) was used to run a numerical simulation on elastic buckling using ANSYS 2021 R1 software to validate the experimental results. The load-displacement relationships and deformed morphologies were investigated using experiments and numerical analysis. The topology arrangement and relative density of the polymer core were examined using the SEM micro-tomography test based on porosity distribution to check the resistance of the sandwich to buckling load. PETG/Al sandwich plates have been found to have critical buckling loads that are 2.52 % higher than PLA/Al sandwich plates, while TPU/Al sandwich plates show increased essential loads of buckling of 5.139 %. The FEM and experiment results show that the existence of porosity in the PLA core in the PFGM plate can reduce the buckling strength tremendously, about 10.52% and 6.8 %, respectively. It was evident that the numerical results show a good agreement with the experimental findings, with a maximum discrepancy of no more than 12 % occurring at the (TPU/Al) sandwich plate with a porosity of 30%.

1 Introduction

The appropriate material selection is a significant challenge in constructing structures that must endure varying loads. The physical and mechanical characteristics of new artificial materials significantly impact their performance and reliability. Functionally graded materials (FGMs) are extensively used as breakthrough structural components for various purposes, including workpiece materials, space systems, energy, dentures, and prosthetics [1]. One of the essential analysis parts of FG plates is the dynamic and static behaviour of such structures, which is particularly useful in various engineering and industrial applications. As a result, several researchers have focused their efforts on this area and presented a review of the FGM developments [2-4].

* Corresponding Author: emad-njim@scrit.gov.iq

Structures with excellent properties, such as lightweight, heat resistance, and energy absorption, have been widely used in various engineering applications [5,6]. Buckling is essential when designing structural members and machine components subjected to compressive loads. When a structural element's length exceeds the other dimensions, it might fail in one of two ways: material yielding or buckling. The part permanently collapses when the load capacity is exceeded. The stability of composite plate structures is extensively examined in terms of analytical, experimental, and numerical results in these studies [7-9]. FGMs can be used to increase the buckling tendency of an element [10, 11].

Therefore, the buckling analysis of FGMs is an attractive subject area. By applying simple higher-order shear deformation theory to porous FG sandwich plates, Daikh and Zenkour [12] analyze the dynamic response. The problem is then modelled using finite element analysis. Based on 3D poroelasticity, Masoud Babaei et al. [13] applied a numerical 3D finite element method to evaluate the natural frequencies and static responses of saturated FG porous annular elliptical sector plates. Kim et al. [14] provided a detailed review of the methodologies used to evaluate buckling behaviours of porous FG microplates using an analytic approach based on generalized coupled stress-based FG porous micro-plates. The Rayleigh-Ritz energy method was used by Masoud Babaei and Kamran Asemi [15] to study the static response of a functionally graded saturated porous rotating truncated cone. Faraz Kiarasi et al. [16] investigated the buckling response of sandwich plates with a polymeric core and two skins strengthened by carbon nanotubes (CNTs) according to higher-order sandwich plate theory. The first shear deformation theory was applied to measure the stability of FGM-reinforced composite plates depending on various thermal and mechanical buckling loads [17]. A novel four-variable shear deformation theory [18] investigated the moisture and heat buckling of size-dependent porous FGM sandwich structures. Various combinations of porosity were used to explore the buckling and free vibration characteristics of sandwich S-FGM plates [19].

Furthermore, the modified Zigzag Theory examined the carbon nanotube-reinforced sandwich plates with functionally graded carbon nanotube reinforcement for bending, free vibration, and buckling [20]. The researchers [21–24] investigated FGM plates' buckling and post-buckling behaviour based on various plate theories. Vinh and Huy [25] studied the buckling characteristics of rectangular plates with porous FGMs using hyperbolic shear deformation theory and FEM. Masoud Babaei et al. [26] examined the dynamic response of a functionally graded saturated porous rotating truncated hollow cone based on 2D axisymmetric poroelasticity. The mathematical model is constructed using the finite element method and minimization of total potential energy. The effects of porosity distribution, Skempton, porosity coefficients, semi-vertex cone angle, and rotational velocity on the stresses and natural frequencies of the structure have been studied. Using the finite element method, Tam et al. [27] investigated the static and dynamic characteristics of an FG graphene-reinforced composite beam with a crack on one side.

Using 3D elasticity theory, Masoud Babaei et al. [28] studied the natural frequencies and dynamic responses of thick annular sector plates and cylindrical plates made of saturated porous materials. Rayleigh-Ritz formulations and Newark methods are used to solve the governing equations. Masoud Babaei et al. [29] investigated stress wave propagation and free vibration response of functionally graded graphene platelets (FG-GPL)-reinforced porous joined truncated conical-cylindrical-conical shell using the Rayleigh-Ritz energy method. Faraz Kiarasi et al. [30] studied the buckling characteristics of FG-saturated porous rectangular plates subjected to normal and shear loads with different boundary conditions (BCs) and porosity distributions. In this study, the GDQ method and finite elements were used in conjunction to develop a computational tool that was efficient in solving the problem. Graphene platelets reinforced truncated conical/cylindrical shells reinforced with functionally graded porous joins were studied by Kiarasi et al. [31]. To solve 2D-axisymmetric elasticity equations, the graded finite element method (GFEM) based on Rayleigh-Ritz energy formulations has been used.

Using higher-order shear deformation theory, Phan Van Vinh [32] examined the bending, free vibration, and buckling behavior of four bidirectional, functionally graded sandwich plate types. Based on the Mindlin plate theory, the phase-field approach is employed to investigate laminates' elastic and buckling behaviour with ply cracks [33].

According to the above literature, most of these studies have focused on theoretical and numerical approaches, particularly the buckling of FGM structures under thermal, mechanical, or mechanical-thermal load behaviour. However, experimental data is scarce, and no research has been reported on porous FG structures.

The primary purpose of this research is to study the stability of porous FGM sandwich plates exposed to compression loads using experimental and FEA methods. According to the power-law distribution, the plate material characteristics may vary gradually only within the plate thickness. As a result, the values of material properties were specified and employed in the buckling analysis. The critical stress of well-designed and fabricated 3D printed FGM plate samples with various metal core types is determined using a PC installed on universal testing equipment (UTM). The second purpose of this paper is to examine how the topology and relative density of the polymer core based on porosity distribution affect the resistance of the sandwich plate to buckling load using the SEM micro-tomography test. Consequently, the article comprehensively examines the porous FGM material and provides helpful analysis and results relevant to applying such materials in the engineering industry.

2 Mathematical Formulation of FGM

The buckling stability of structural components is one of the most critical parameters in structural design. According to the power-law distribution, the plate material characteristics may vary gradually only within the plate thickness. As a

result, the values of material properties were specified and employed in the buckling analysis. This section defines a rectangular plate primarily made of a functionally graded material; however, the plate was supposed to be constructed of two different material phases, such as metal and ceramic. The combination with the volume fractions of metal and ceramic is expressed as [34],

$$V_1(z) + V_2(z) = 1 \quad (1)$$

V_1 and V_2 are ceramic and metal volume fractions on the bottom and top surfaces. The composite material is spatially isotropic, with mechanical properties that vary gradually only in the z -direction. The following power-law function is considered to determine the grading of the volume fraction of the ceramic phase from the bottom to top plate surfaces,

$$V_1(z) = \left(\frac{z+\frac{h}{2}}{h}\right)^n \quad (2)$$

The material property at a point of the FG plate can be found as,

$$U(z) = (U_1 - U_2) \left(\frac{z+\frac{h}{2}}{h}\right)^n + U_2 \quad (3)$$

U_1 and U_2 represent the mechanical characteristics of the ceramic and metal elements, respectively; n is a power-law variation index, in which $n \in [0, \infty)$. A ceramic plate has a value of zero n , but an utterly metallic plate has a value of infinite (n) [35].

The plate in the current work is intended to comprise only one metal with density changes over its thickness. As a result, it serves as an FGM component. As a consequence, the proposed volume fraction rule is as follows,

$$V_p(z) = V_2 - V_2\eta \left(\frac{z}{h} + \frac{1}{2}\right)^n \quad (4)$$

For, $n = 0$, $V(z) = V_2 - \eta V_2$, while for; $n = \infty$, $V_p = V_2 = 1$. V_p denotes the entire volume of porous metal, while V_2 represents the volume of core metal, and η is the porosity factor. However, the material characteristics of the porous FGM plate throughout all features of the suggested mathematical model can be expressed as follows,

$$U(z) = U_2 - \eta \cdot U_2 \left(\frac{z}{h} + \frac{1}{2}\right)^n \quad (5)$$

For our current formulations, the mechanical characteristics, such as the elastic modulus (E) and mass density (ρ), are assumed to change in the thickness direction, except for Poisson's ratio (ν), which will be kept constant for convenience, based on previous studies such as Czechowski and Kołakowski [36]. Consider a uniformly thin, linearly elastic rectangular FG plate, as depicted in Figure 1.

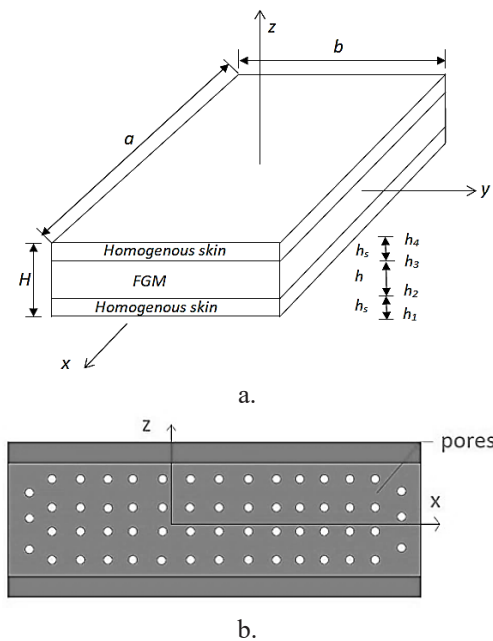


Fig. 1. (a) the schematic of a sandwich plate composed of an FG core and two homogenous skins, (b) Even porosity distribution across the core thickness.

Within the core metal phase, the imperfect FGM core with porosity ($\eta < 1$) is evenly distributed [37]. The FG plate has dimensions of length a and width b , with lower and upper skins composed of the same homogeneous material and

thickness (i.e., $h_{s1}=h_{s2}$, $E_{s1} = E_{s2} = E_s$, $\nu_{s1} = \nu_{s2} = \nu$, $\rho_{s1} = \rho_{s2} = \rho_s$). The density and modulus elasticity of the porous FG plate can be written as,

$$\rho(z) = \rho_2 - \eta \cdot \rho_2 \left(\frac{z}{h} + \frac{1}{2} \right)^n \quad (6)$$

$$E(z) = E_2 - \eta \cdot E_2 \left(\frac{z}{h} + \frac{1}{2} \right)^n \quad (7)$$

By performing multiple integrations along with the sandwich plate thickness, the flexural rigidity D_{FG} and inertia I_{FG} of the FG sandwich plate can be found in the following form [21],

$$D_{FG} = \frac{E_2 h^3}{12(1-\nu^2)} - \frac{\eta E_2 h^3}{(1-\nu^2)} \left(\left(\frac{1}{(n+3)} - \frac{1}{(n+2)} + \frac{1}{4(n+1)} \right) + \frac{E_s}{(1-\nu^2)} \left(\frac{2 \left(\frac{h}{2} + h_s \right)^3}{3} - \frac{h^3}{12} \right) \right) \quad (8)$$

$$I_{FG} = \rho_2 h \left(1 - \frac{\eta}{(n+1)} \right) + 2\rho h_s \quad (9)$$

3 Experimental Work

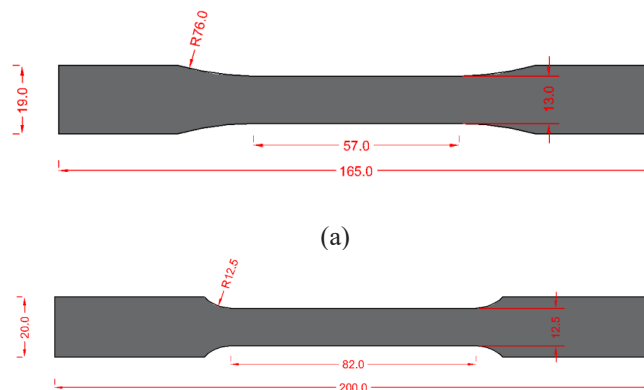
The experimental program includes selecting the materials used, designing the specimens with various porosities, and performing tensile and compression tests.

3.1 Materials

Gradients of porosity can be achieved in functionally gradient materials by changing the spatial position. The effect of this can be achieved by using 3D printing technology. This component varies in density through the layers of the part. Polylactic Acid (PLA), Thermoplastic Polyurethane (TPU), and Polyethylene Terephthalate with Glycol (PETG) are three types of polymers used in this work, developed by FlashForge (Hangzhou, Zhejiang, China). Every polymer was with a standard wire diameter of 1.75 mm. Each has unique characteristics and applications that set it apart from the different types. A 3D printing method was used to fabricate samples for tensile and buckling testing.

3.2 The Tensile Test

Tensile properties determine which materials should be selected. Material specifications often specify tensile properties, so testing is needed to ensure the materials meet these properties. The dimensions of both specimens and the photo geometry are depicted in Figure 2. ASTM standard D638 [38] was used for the polymer sample production, while ASTM standard E 8M-00b [39] was used for the aluminium sample production. With the help of a Spectrometer device type (ARC.MET 8000), we were able to determine the [chemical composition of aluminium alloy \(AA6061-T6\)](#) under ASTM E1251-94 [40]. Table 1 lists the results, which are within standard parameters. According to Figure 4, microcomputer-controlled electronics tested the uniaxial tensile strength of the Tinius Olsen H50KT apparatus using a universal testing machine (UTM) [with a maximum applied force of 50 KN](#). The tensile strength of metals and polymers has been limited. In order to measure accuracy further, six readings were taken for each polymer type and three for the aluminium sample. See Table 2. The stress-strain curves of PLA samples are shown in Figure 5.



(b)

Fig. 2. Tensile specimen sketch per ASTM, a. (D638), b. (E 8M-00b) (all dimensions in mm).



Fig. 3. The 3D printing method was used to manufacture polymer tensile test samples



Fig. 4. Specimen during tensile test.

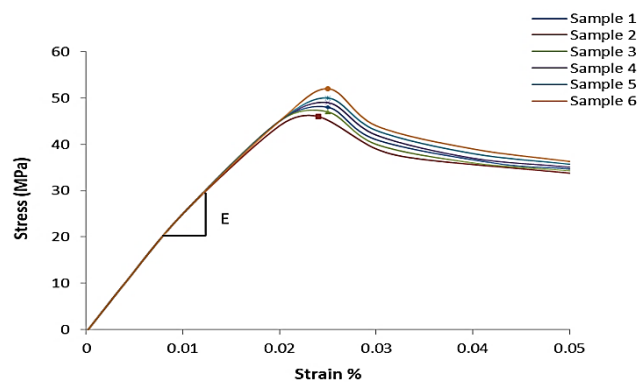


Fig.5. Stress-strain curve for PLA samples.

3.3 Manufacturing of the FG Sandwich plates

There are four porosity parameters in the samples, exhibiting a thickness of 1 mm, three porosity parameters, and three bonding parameters. Testing is conducted on all of these using a universal testing machine (Tinius Olsen H50KT). The maximum compression load and total deflection are reported based on test results obtained using the testing instrument's programmable controller (PC). The CR-10 Max 3D printer was used to fabricate all the tested samples

using a model of pore size designed in Solid Works as a (.stl) file and then used for printing the model through Solid Works. For the current work, an aluminium plate with a thickness of (1 mm) was used as the face sheet material, selected as the most widely used for engineering applications and aerospace structures. Figure 7 illustrates that on the face sheet's top and bottom surfaces, exceptional adhesion (Epoxy) is used to bond the face sheet to the FG core.



Fig. 6. Manufacturing FG specimens using 3-D printing

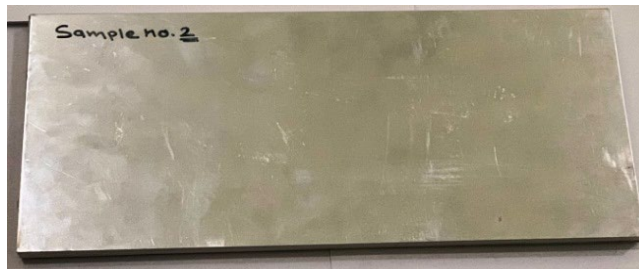


Fig. 7. Preparation for FG plate specimens

Table 1. The chemical analysis of Aluminum alloy (wt%)

Mg	Mn	Si	Fe	Cr	Cu	Ti	Zn	Al
0.85	0.106	0.44	0.58	0.04	0.14	0.23	0.008	Bal.

Table 2. Material properties of sandwich plates resulted from tensile test.

Material	Tensile strength (MPa)	Yield strength (MPa)	E (GPa)
PLA	46	40.2	1.2
TPU	38	40	0.8
PETG	52	44	2.1
AA6061-T6	350	312	71.56

3.4 Experimental Procedures for Buckling Test

Buckling experiments measured the buckling behaviour of sandwich plates constructed of functionally graded porous metal. The test samples used in the study were made of Functionally Graded Material (FGM) with dimensions of 150 mm * 300 mm. The specimens had different core heights, specifically 5 mm, 10 mm, 15 mm, 20 mm, and 25 mm. During the experiment, the samples were subjected to simply supported-fixed-supported-fixed (SFSF) boundary conditions, where the plate was attached to fixtures.

All experiments were conducted using an electromechanical universal testing machine (UTM). The specimens were compressed in a unidirectional manner at a displacement-controlled rate of 0.5 mm/min along the y-axis direction. The force-extension curve, obtained by the UTM, was utilized to determine the critical buckling loads for the plate structure, as shown in Figure 8.

A test of identical properties was conducted thrice on samples to ensure accuracy.

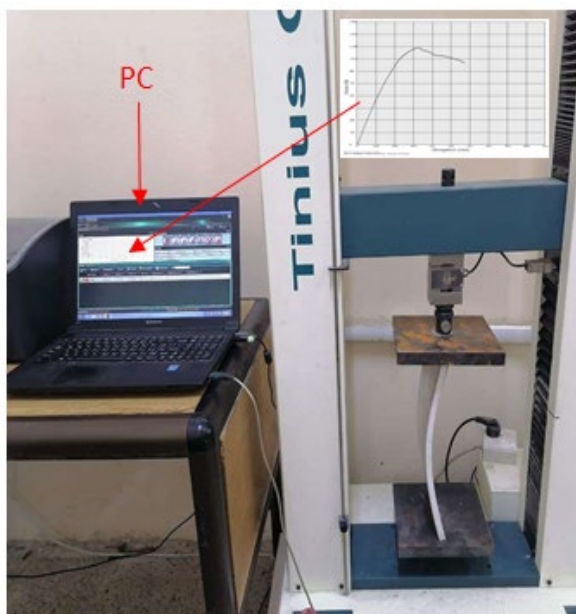


Fig. 8. The FG plates during the buckling test.

3.5 Finite Element Modeling

Numerical techniques are typically employed to validate the precision of the experimental solution [41-44]. There are several mathematical approaches to solving issues, but the FEA method is the most accurate. This study used conventional eigenvalue buckling analysis to estimate the critical buckling loads using an FE model constructed and analyzed with ANSYS Workbench software (Version 2021 R1). The geometry and material properties of the problem are considered as $a= 0.5$ (m) and $b= 0.5$ (m), various core thicknesses, while the skins have 1 mm each. Figure 9 shows a 3D rectangular sandwich plate model, while Figure (10) illustrates the meshed model with 8-node SOLID186 components using the fine grid size under uniaxial loading conditions.

This simulation case generated a mesh size of 0.5 mm, 192,809 nodes, and 40000 elements. By using Table (2) and Equations (6,7), the material characteristics of the porous core were given to the geometries with the elastic modulus (E) and Poisson’s ratio (ν) for each instance and then inserted into the FE simulation model using Excel 2019 program. The mechanical characteristics of skins are presented in Table 3. First, a linear static analysis for edge loads equal to 1 N was performed on the porous FG samples in a static structural environment, and then the solution was transferred to an Eigenvalue buckling analysis. As a result of buckling analysis in ANSYS, the Eigenvalue technique or nonlinear static analysis may be carried out. Eigenvalue buckling simulation determines the buckling strength in linear and nonlinear static analysis. The buckling of the elastic framework can be defined by linear eigenvalue buckling analysis, which provides flexible assumptions for later analysis of nonlinear structures.

A total deformation buckling load and mode shapes were then calculated through compression load and boundary conditions on the edges, thereby identifying the critical buckling load of the FGM sandwich. The current numerical analyses considered five types of boundary conditions, including four edges clamped (CCCC), three edges clamped, and one is free (CCCF), two edges simply supported and other two edges clamped (SCSC), all four edges simply-supported (SSSS), and finally three clamped edges with one simply supported (CCCS).

Table 3. Material properties of the sandwich plates [45].

Polymer	Young Modulus (GPa)	Mass Density (kg/m ³)	Poisson ratio
PEEK 30 % CF	7.69	1414	0.42
ABS	2.52	1428	0.41
PBT	2.68	1347	0.40

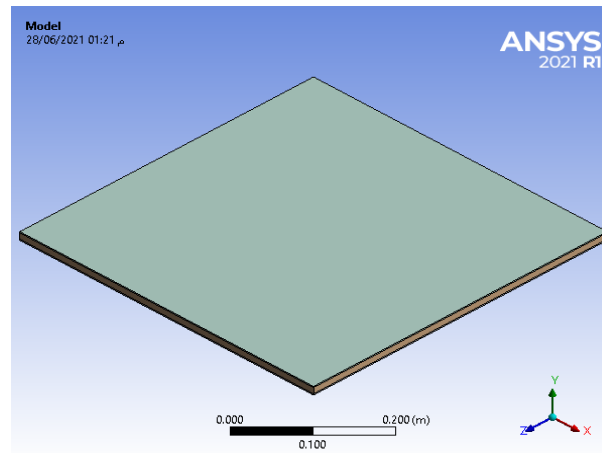


Fig. 9. Simulation process for the FG model.

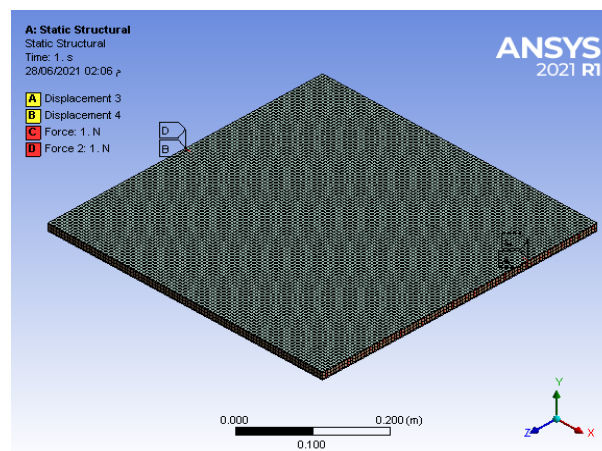


Fig. 10. Meshing the model for the SFSF BCs.

4 Results And Discussion

An analysis of crucial problem characteristics is provided in this section. Consequently, a non-dimensional buckling load parameter was employed [8],

$$\bar{N} = N_{x,cr} \frac{a^2}{E_p H^3} \quad (10)$$

Table 4 and Figure 11 present experimental and numerical results for the critical buckling load of a sandwich plate composed of PLA core and (Al) skins. A fixed power-law index ($n=1$) and various porosity factors are used to compare. Three slenderness ratios ($a/H = 30, 20, 15$) and an aspect ratio ($b/a = 0.5$) are considered to determine the effect of decreasing geometrical parameters on the critical load.

The experimental and numerical results show good agreement, with a maximum discrepancy of 9.51% observed for the slenderness ratio ($a/H = 30$) and porosity factor ($\eta = 0$). This confirms the reliability of the 3-D FG finite element model used. Furthermore, it is observed that a higher porosity content leads to a lower critical buckling load. Additionally, the critical buckling load increases as the side-thickness ratio increases.

It can be inferred that both geometrical and porosity properties play a significant role in determining the overall stiffness of the plate.

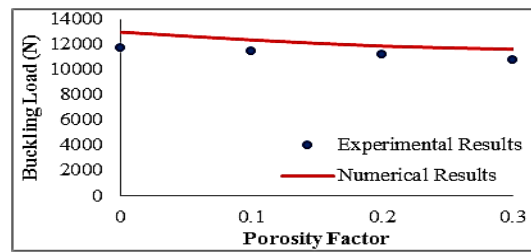
In Table 5 and Figure 12, we show the effect of PETG porous metal on sandwich plate stability. Experimental results are significantly different from those in Table 4. This study found the most significant error percentage between experimental and numerical results when a/H was 30 and porosity was 0.3. In addition to being extraordinarily impact-resistant and pliable, PETG polymer has extremely low shrinkage, so it is an excellent choice for components. It has also been found that the plates are deformed at their centers as the height-to-thickness ratio increases.

As shown in Tables 6 and 13, the SFSF sandwich plate composed of TPU can withstand various critical buckling loads. Metal that is porous and made up of thermoplastic polyurethane. The UTM and simulation results exhibit significant agreement, with a maximum % error percentage of 12% observed at a slenderness ratio of $a/H = 30$ and a porosity factor of $\eta = 0.3$. Similar trends are kept in the results presented in Table 6, as in Tables 4 and 5. Based on these findings, it can be concluded that TPU is a versatile material suitable for various applications, including car

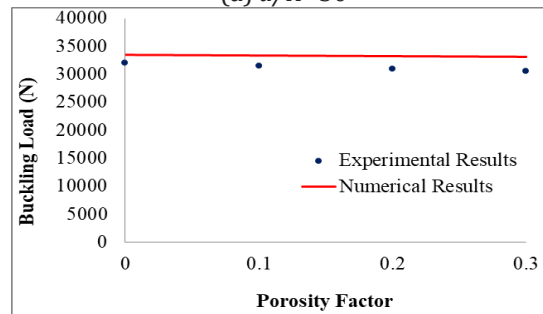
instrument panels and medical devices. The results suggest that TPU possesses properties that make it ideal for these specific applications.

Table 4. The effect of skin thickness and b/a ratio on the buckling loads (N) of SFSF sandwiches (PLA/Al), adapted to 1mm skin thickness and b/a ratio =0.5.

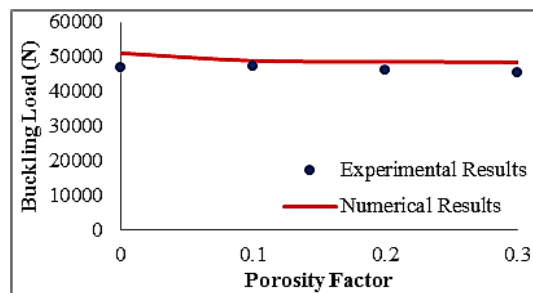
a/H	η	Exp.	Num.	Error (%)
30	0	11750	12984.924	9.51
	0.1	11480	12362.883	7.14
	0.2	11179	11870.840	5.83
	0.3	10950	11618.802	5.76
20	0	32100	33514.204	4.22
	0.1	31550	33396.080	5.53
	0.2	31000	33277.955	6.85
	0.3	30645	33159.831	7.58
15	0	46800	51068.118	8.36
	0.1	46450	48856.621	4.93
	0.2	46185	48645.125	5.06
	0.3	45354	48433.628	6.36



(a) $a/H=30$



(b) $a/H=20$



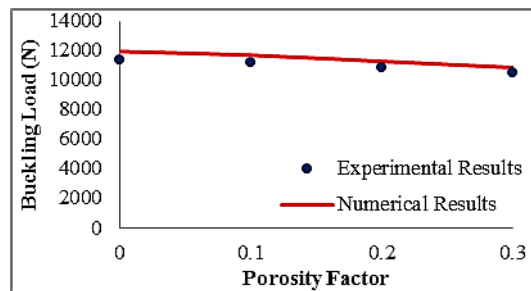
(c) $a/H=15$

Fig. 11. Experimental and numerical buckling results for (PLA/Al) PFG plates.

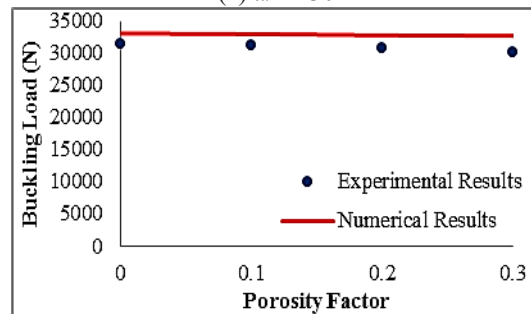
Table 5. SFSF sandwich (PETG/Al), skin thickness 1mm, $b/a=0.5$, experimental and numerical investigation of buckling loads (N).

a/H	η	Exp.	Num.	Error (%)
30	0	11400.11	11950.125	4.60
	0.1	11190.10	11695.624	4.32
	0.2	10838.09	11277.124	3.89
	0.3	10535.08	10858.623	2.98
20	0	31560	33134.764	4.75
	0.1	31175	33035.612	5.63
	0.2	30867	32836.459	5.99
	0.3	30189	32737.307	7.78

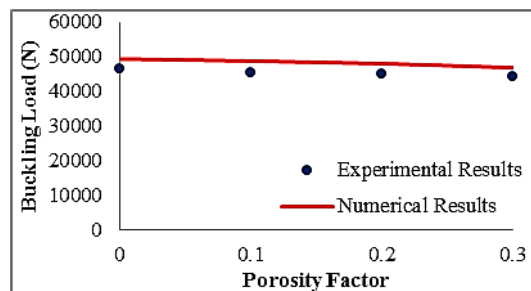
15	0	46450	49388.747	5.95
	0.1	45370	48811.220	7.05
	0.2	44845	48033.692	6.64
	0.3	44250	46856.164	5.56



(a) $a/H=30$



(b) $a/H=20$



(c) $a/H=15$

Fig. 12. Experimental and numerical buckling results for (PETG/Al) sandwich plate.

Table 6. The variation in buckling loads (N) for SFSF sandwich panels (TPU/Al) with a skin thickness of 1mm and a ratio of $b/a=0.5$ was investigated experimentally and numerically.

a/H	η	Exp.	Num.	Error (%)
30	0	11200	11665.2	3.98
	0.1	10890	11635.38	6.41
	0.2	10455	11621.87	10.04
	0.3	10180	11568.37	12.00
20	0	27175	28165.52	3.52
	0.1	26490	27982.29	5.33
	0.2	26750	27924.33	4.21
	0.3	26110	27866.37	6.30
15	0	45189	46902.17	3.65
	0.1	44165	46730.34	5.49
	0.2	43580	46700.72	6.68
	0.3	42950	45125.92	4.82

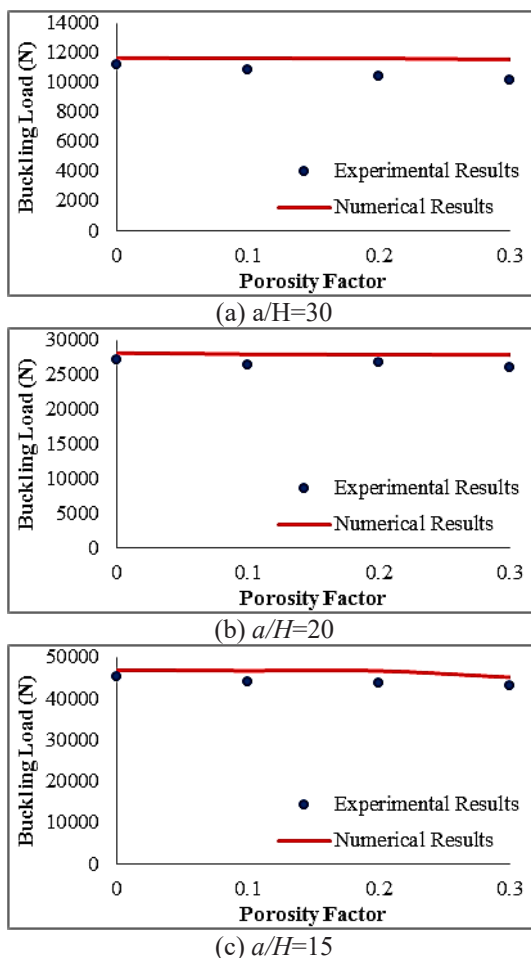


Fig. 13. Comparison of experimental and numerical buckling results for (TPU./Al) sandwich plate.

FG sandwich plates with PLA cores, 50/50 aspect ratios, and 1.0 mm skin thickness are modelled with five boundary conditions, as shown in Figure 14. Variation indexes are being studied for their influence. According to the findings, plate buckling characteristics increase with boundary condition constraint; **fixed from all edges (CCCC)** has a more significant buckling coefficient than CCCS. The circumstances of this case are much more severe than those of the SCSC.

As shown in Figure 15, for a square porous functionally graded plate with $a/H = 50$, buckling load parameters are calculated using several core metals, including PEEK 30 % CF, PBT, TPU, ABS, PETG, and PLA. PLA core-type buckling loads are higher than other types because PEEK 30%CF and material properties are lower. Since its mechanical properties are high (it is stiffer than all different types), as a result, it is used in a variety of industrial and construction settings.

Table 7 and Figure 16 display a rectangular sandwich plate's non-dimensional buckling load data. The plate has an aspect ratio of $a/h = 50$ and is subjected to various porosity factors ($\eta = 0.1, 0.2, 0.3, 0.4,$ and 0.5), volume fraction indexes ($n = 0, 0.5, 1.2, 5, 10,$ and 100), and aspect ratios of 0.25, 0.5, 0.75, and 2. These data provide a comprehensive overview of the buckling load behaviour for different combinations of these factors. It is noticed that the buckling load parameters decrease with increasing porosity and increase with increasing gradient index and aspect ratio. In other words, reduced material rigidity may be responsible for this. In addition, the power-law index (n) was not significantly different from 50 when buckling load was determined.

Fractured surfaces on a graded sample at different working distances (WD) and porosity levels of 0.1 and 0.3 were examined using SEM. Figures 17 and 18 display these surfaces, showcasing the absence of striations but the presence of grain boundaries and melt pool boundaries with varying local orientations.

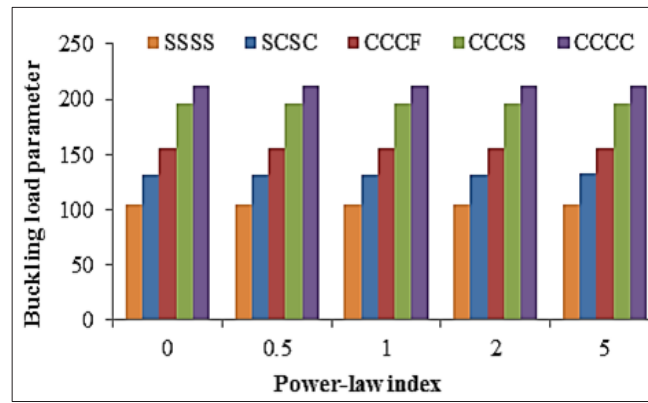


Fig.14. Influence of BCs on Buckling Load

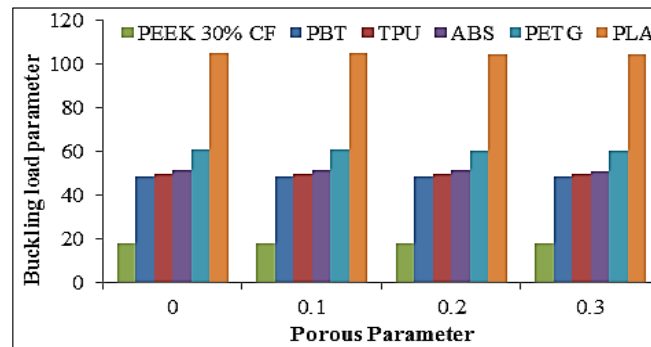
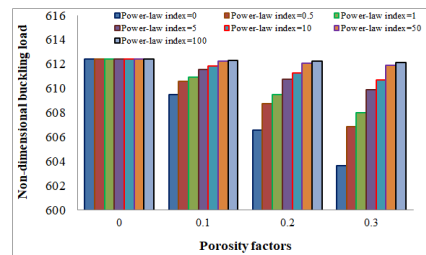
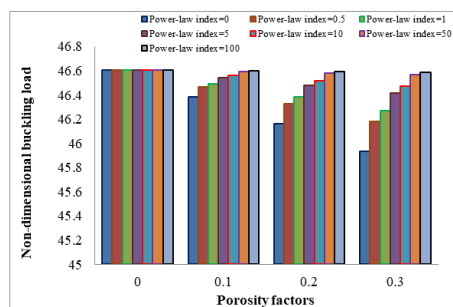


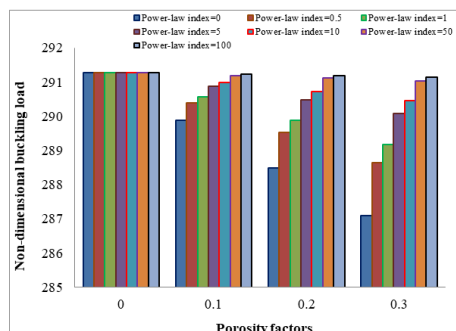
Fig. 15. The impact of core metal on bucking characteristics



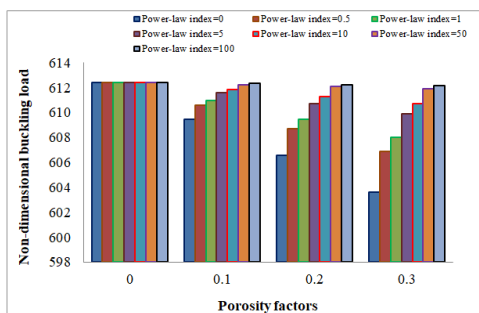
(a) $b/a=0.25$



(b) $b/a=0.5$



(c) $b/a=0.75$



(d) $b/a=1$

Fig. 16. Non-dimensional buckling parameter of the SSSS plate with PLA with different porosity factors effect.

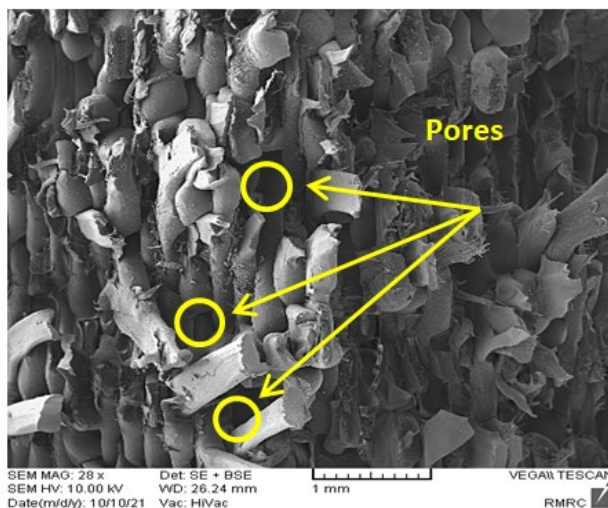


Fig. 17. SEM images of bending fracture surface of FGM sample at porosity 10%, and gradient index $n=1$.

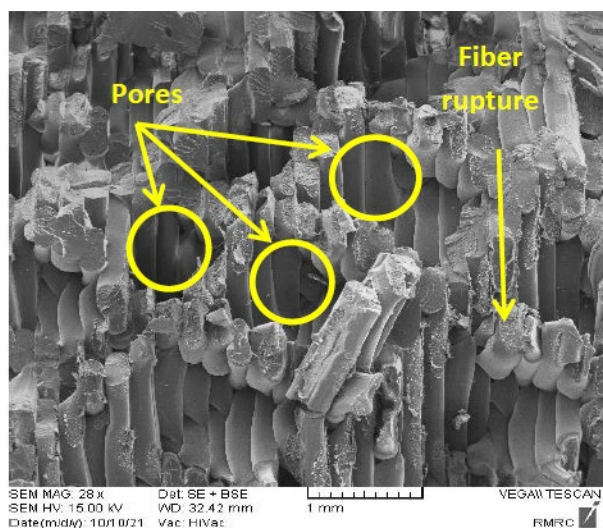
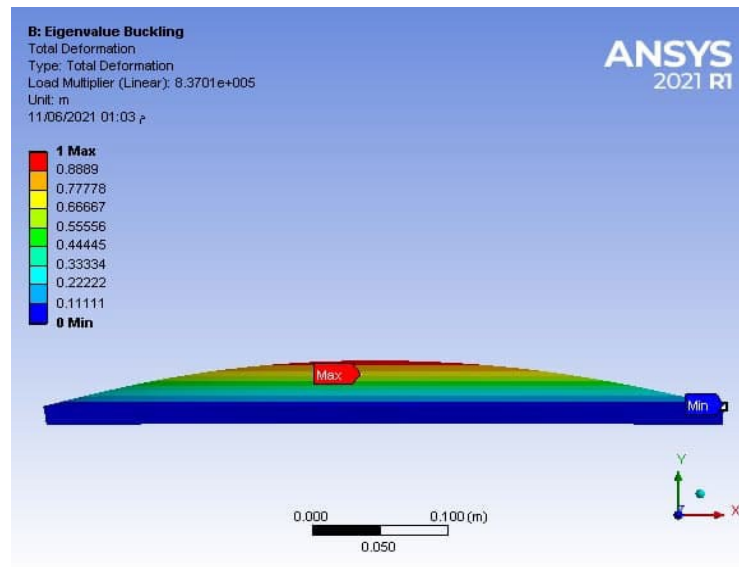
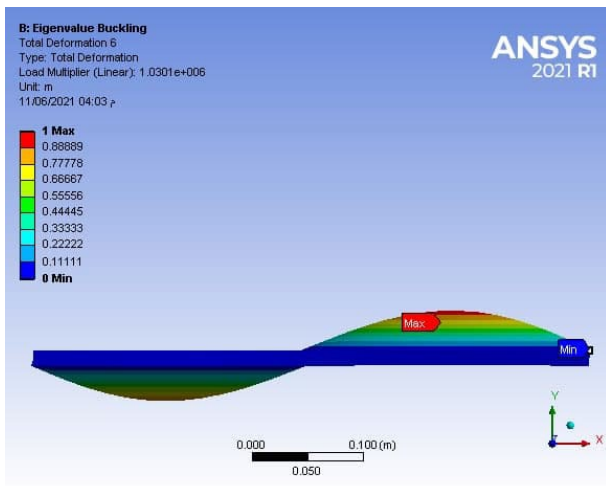


Fig. 18. SEM images of bending fracture surface of FGM sample at porosity 20%, and gradient index $n=1$

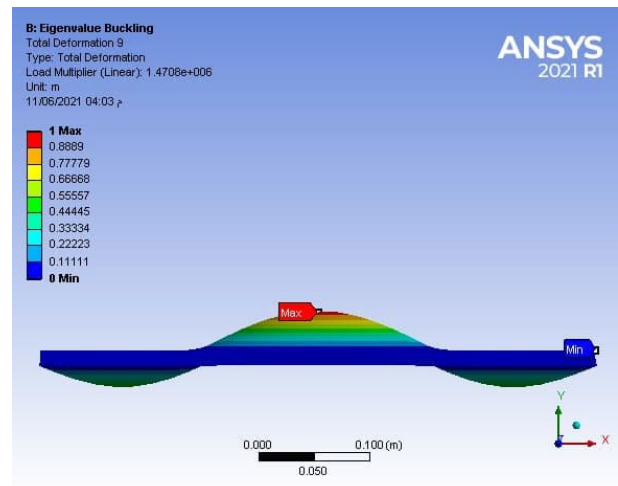
Figure 19 illustrates the three-dimensional numerical buckling mode shapes of an SSSS FG square sandwich plate (PLA/Al) with $\eta = 0.25$ and $n = 2$ conducted by ANSYS software tools. The 1st mode shape describes a deformation due to bending; lateral, 2nd, and 3rd modes have identical profiles; the 4th mode indicates a torsional mode, while the 5th and 6th modes have different shapes.



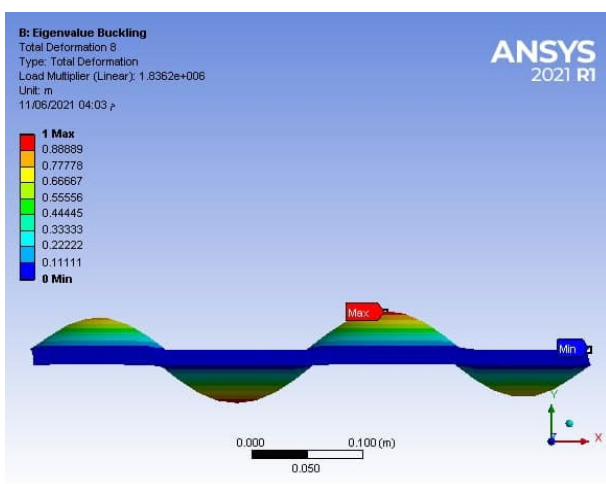
a. Mode-1



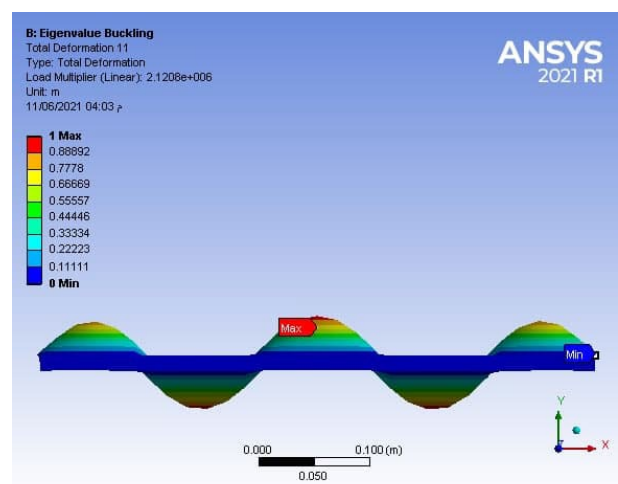
b. Mode-2



c. Mode-3



d. Mode-5



e. Mode-5

Fig. 19. The first six buckling modes show a square SSSS sandwich plate with a PLA core ($\eta=0.2$, $n=2$, $h_s = 1$ mm).

Table 7. Analysis of SSSS plates with PLA cores and Aluminum skins with non-dimensional parameters (h_c 10 mm h_s 1mm).

b/a	η	Power-law index, n						
		0	0.5	1	5	10	50	100
0.25	0	18.204	18.204	18.204	18.204	18.204	18.204	18.204
	0.1	18.118	18.150	18.161	18.180	18.187	18.200	18.202
	0.2	18.031	18.095	18.118	18.155	18.170	18.195	18.199
	0.3	17.944	18.041	18.074	18.130	18.153	18.190	18.197
0.5	0	46.603	46.603	46.603	46.603	46.603	46.603	46.603
	0.1	46.381	46.463	46.492	46.540	46.560	46.591	46.597
	0.2	46.159	46.324	46.381	46.476	46.516	46.579	46.590
	0.3	45.936	46.184	46.270	46.413	46.473	46.567	46.584
0.75	0	291.269	291.269	291.269	291.269	291.269	291.269	291.269
	0.1	289.880	290.396	290.575	290.872	290.997	291.194	291.230
	0.2	288.491	289.523	289.880	290.475	290.725	291.118	291.190
	0.3	287.101	288.649	289.185	290.079	290.453	291.042	291.150
1	0	612.394	612.394	612.394	612.394	612.394	612.394	612.394
	0.1	609.473	610.558	610.933	611.559	611.822	612.235	612.311
	0.2	606.552	608.722	609.473	610.725	611.250	612.076	612.227
	0.3	603.630	606.885	608.012	609.890	610.678	611.917	612.144

5 Conclusions

The main purpose of this research is to study the stability of porous FGM sandwich plates exposed to compression loads using experimental and FEA methods. The buckling analyses of the PFGM sandwich plate subjected to uniaxial loading are presented in this work using a testing program. The mixture rule calculates the appropriate mechanical properties of the PFGM. Different finite element models are generated and analyzed using the FEA program ANSYS 2021 R1 to anticipate experimental results. Thus, the buckling characteristics of the sandwich plate with various core materials, porosity distributions, and geometrical factors are demonstrated. The comprehensive numerical findings, including critical buckling loads, are reported in non-dimensional parameters. The article thoroughly examines the porous FGM material and provides helpful analysis and results relevant to applying such materials in the engineering industry. The following conclusions can be described as,

1. At an aspect ratio of 0.5 and a thickness ratio of 30, the critical buckling loads change from (PLA/Al) to (PETG/Al), while they increase from (2.52) % to (5.140) % when (TPU/Al) sandwich structure is used. This type performs better than all the polymers employed in the investigation.
2. The buckling parameter increases by (1.42) % at $\eta=30\%$ when the gradient index changes from $n=0$ to $n=100$.
3. The tables and figures indicate that, regardless of the boundary conditions employed, porosity distributions play a critical role in determining eigenvalue buckling characteristics and, as a result, identifying the stability of the FG sandwich plates.
4. A reasonable agreement was established between the experimental and finite element analysis using ANSYS software for buckling analysis, with a percentage error of no more than 15%, indicating that there was no delamination between the layers of FGM samples and that the test samples were well-fabricated.
5. PETG is an excellent polymer for high-impact mechanical parts subjected to buckling loads. Hence, this type is widely used in aircraft applications.
6. The SEM results show that porosity distribution will influence fiber orientation and rupture more. However, the fracture surface can indicate fibers with different local orientations in adjacent regions or melt pool boundaries

Nomenclature

V_1	The volume fraction of ceramic
V_2	The volume fraction of metal
n	Power-law index
h	Plate height (m)
h_c	Core thickness (mm)
$U(z)$	The material properties of FGM
U_1	A material property of FGM lower surface
U_2	The material property of FGM upper surface
V_p	The volume fraction of porous metal
a,b	Plate length and width (m)

E_{s1}, E_{s2}	Modulus elasticity of upper and lower skins (GPa)
hs_1, hs_2	The thickness of upper and lower skins (m)
E	Modulus elasticity (GPa)
DFG	Flexural rigidity of the plate
IFG	Inertial coefficient (kg/m ²)
PFG	Porous functionally graded
Greek Symbols	
ρ	Density (kg/m ³)
η	Porosity parameter
ν	Poisson's ratio
ν_{s2}, ν_{s1}	Poisson's ratio of upper and lower skins
Subscripts	
s	skin
p	Porous
FG	Functionally graded

References

1. E. K. Njim, S. H. Bakhy, and M. Al-Waily, "Analytical and numerical free vibration analysis of porous functionally graded materials (FGPMs) sandwich plate using Rayleigh-Ritz method," *Archives of Materials Science and Engineering*, vol. 1, no. 110. Index Copernicus, pp. 27–41, Jul. 01, 2021. doi: 10.5604/01.3001.0015.3593.
2. B. Saleh et al., "30 Years of functionally graded materials: An overview of Manufacturing Methods, Applications and Future Challenges," *Composites Part B: Engineering*, vol. 201. Elsevier BV, p. 108376, Nov. 2020. doi: 10.1016/j.compositesb.2020.108376.
3. A. Garg, M. O. Belarbi, H. D. Chalak, and A. Chakrabarti, "A review of the analysis of sandwich FGM structures," *Composite Structures*, vol. 258. Elsevier BV, p. 113427, Feb. 2021. doi: 10.1016/j.compstruct.2020.113427.
4. A. Mouthanna, S. H. Bakhy, M. Al-Waily, and E. K. Njim, "Free Vibration Investigation of Single-Phase Porous FG Sandwich Cylindrical Shells: Analytical, Numerical and Experimental Study," *Iranian Journal of Science and Technology, Transactions of Mechanical Engineering*. Springer Science and Business Media LLC, Aug. 29, 2023. doi: 10.1007/s40997-023-00700-7.
5. F. Kiarasi, M. Babaei, P. Sarvi, K. Asemi, M. Hosseini, and M. Omidi Bidgoli, "A review on functionally graded porous structures reinforced by graphene platelets," *J Appl. Comput. Appl. Mech.*, vol. 52, no. 4, Dec. 2021, doi: 10.22059/jcamech.2021.335739.675.
6. M. Babaei, K. Asemi, P. Safarpour, "Natural Frequency and Dynamic Analyses of Functionally Graded Saturated Porous Beam Resting on Viscoelastic Foundation Based on Higher Order Beam Theory," *Journal of Solid Mechanics*, vol. 11, no. 3, pp. 615-634, 2019. DOI: 10.22034/JSM.2019.666691
7. M. Al-Waily, M. J. Jweeg, M. A. Al-Shammari, K. K. Resan, and A. M. Takhakh, "Improvement of Buckling Behavior of Composite Plates Reinforced with Hybrids Nanomaterials Additives," *Materials Science Forum*, vol. 1039. Trans Tech Publications, Ltd., pp. 23–41, Jul. 20, 2021. doi 10.4028/www.scientific.net/msf.1039.23.
8. E.K. Njim, S.H. Bakhy, M. Al-Waily, "Analytical and Numerical Investigation of Buckling Behavior of Functionally Graded Sandwich Plate with Porous Core," *Journal of Applied Science and Engineering* vol. 25, no. 2, Apr. 2022, doi: 10.6180/jase.202204_25(2).0010.
9. Y. Sitli, K. Mhada, O. Bourihane, and H. Rhanim, "Buckling and post-buckling analysis of a functionally graded material (FGM) plate by the Asymptotic Numerical Method," *Structures*, vol. 31. Elsevier BV, pp. 1031–1040, Jun. 2021. doi: 10.1016/j.istruc.2021.01.100.
10. H. Yaghoobi and F. Taheri, "Analytical solution and statistical analysis of buckling capacity of sandwich plates with uniform and non-uniform porous core reinforced with graphene nanoplatelets," *Composite Structures*, vol. 252. Elsevier BV, p. 112700, Nov. 2020. doi: 10.1016/j.compstruct.2020.112700.
11. M. Babaei, K. Asemi, and P. Safarpour, Buckling and Static Analyses of Functionally Graded Saturated Porous Thick Beam Resting on Elastic Foundation Based on Higher Order Beam Theory, *Iranian Society of Mechanical Engineering*, vol. 20, no. 1, pp. 94-112, 2019.
12. A. A. Daikh and A. M. Zenkour, "Free vibration and buckling of porous power-law and sigmoid functionally graded sandwich plates using a simple higher-order shear deformation theory," *Materials Research Express*, vol. 6, no. 11. IOP Publishing, p. 115707, Oct. 11, 2019. doi: 10.1088/2053-1591/ab48a9.
13. M. Babaei, K. Asemi, and F. Kiarasi, "Static response and free-vibration analysis of a functionally graded annular elliptical sector plate made of saturated porous material based on 3D finite element method," *Mechanics Based*

- Design of Structures and Machines, vol. 51, no. 3. Informa UK Limited, pp. 1272–1296, Dec. 30, 2020. doi: 10.1080/15397734.2020.1864401.
14. J. Kim, K. K. Żur, and J. N. Reddy, “Bending, free vibration, and buckling of modified couples stress-based functionally graded porous micro-plates,” *Composite Structures*, vol. 209. Elsevier BV, pp. 879–888, Feb. 2019. doi: 10.1016/j.compstruct.2018.11.023.
 15. M. Babaei and K. Asemi, “Stress analysis of functionally graded saturated porous rotating thick truncated cone,” *Mechanics Based Design of Structures and Machines*, 2020. DOI: 10.1080/15397734.2020.1753536
 16. Kiarasi F., Babaei M., Dimitri R., et al., “Hygrothermal modeling of the buckling behavior of sandwich plates with nanocomposite face sheets resting on a Pasternak foundation,” *Continuum Mech. Thermodyn*, vol. 33, pp. 911–932, 2021. DOI: 10.1007/s00161-020-00929-6
 17. J.F. Wang, S.H. Cao, W. Zhang, “Thermal vibration and buckling analysis of functionally graded carbon nanotube reinforced composite quadrilateral plate,” *European Journal of Mechanics-A/Solids*, vol. 85, 2021. DOI: 10.1016/j.euromechsol.2020.104105
 18. M. Sobhy, “Size-dependent hygro-thermal buckling of porous FGM sandwich microplates and microbeams using a novel four-variable shear deformation theory,” *International Journal of Applied Mechanics*, vol. 12, no. 2, 2020. DOI: 10.1142/S1758825120500179
 19. S.J. Singh, S.P. Harsha, “Buckling analysis of FGM plates under uniform, linear and nonlinear in-plane loading,” *Journal of Mechanical Science and Technology*, vol. 33, pp. 1761–1767, 2019. DOI: 10.1007/s12206-019-0328-8
 20. MD. Sciuva, M. Sorrenti, “Bending, free vibration and buckling of functionally graded carbon nanotube-reinforced sandwich plates, using the extended Refined Zigzag Theory,” *Composite Structures*, vol. 227, 2019. DOI: 10.1016/j.compstruct.2019.111324
 21. C. Li, H.-S. Shen, H. Wang, and Z. Yu, “Large amplitude vibration of sandwich plates with functionally graded auxetic 3D lattice core,” *International Journal of Mechanical Sciences*, vol. 174. Elsevier BV, p. 105472, May 2020. doi: 10.1016/j.ijmecsci.2020.105472.
 22. V. N. Burlayenko and T. Sadowski, “Free vibrations and static analysis of functionally graded sandwich plates with three-dimensional finite elements,” *Meccanica*, vol. 55, no. 4. Springer Science and Business Media LLC, pp. 815–832, Jul. 01, 2019. doi: 10.1007/s11012-019-01001-7.
 23. S. Singh and S. Harsha, “Analysis of porosity effect on free vibration and buckling responses for sandwich sigmoid function based functionally graded material plate resting on Pasternak foundation using Galerkin Vlasov’s method,” *Journal of Sandwich Structures & Materials*, vol. 23, no. 5. SAGE Publications, pp. 1717–1760, Feb. 10, 2020. doi: 10.1177/1099636220904340.
 24. M. Babaei, K. Asemi, and F. Kiarasi, “Dynamic analysis of functionally graded rotating thick truncated cone made of saturated porous materials,” *Thin-Walled Structures*, vol. 164. Elsevier BV, p. 107852, Jul. 2021. doi: 10.1016/j.tws.2021.107852.
 25. M. Arefi and F. Najafitabar, “Buckling and free vibration analyses of a sandwich beam made of a soft core with FG-GNPs reinforced composite face-sheets using Ritz Method,” *Thin-Walled Structures*, vol. 158. Elsevier BV, p. 107200, Jan. 2021. doi: 10.1016/j.tws.2020.107200.
 26. P. Van Vinh and L. Q. Huy, “Finite element analysis of functionally graded sandwich plates with porosity via a new hyperbolic shear deformation theory,” *Defence Technology*, vol. 18, no. 3. Elsevier BV, pp. 490–508, Mar. 2022. doi: 10.1016/j.dt.2021.03.006.
 27. M. Tam, Z. Yang, S. Zhao, and J. Yang, “Vibration and Buckling Characteristics of Functionally Graded Graphene Nanoplatelets Reinforced Composite Beams with Open Edge Cracks,” *Materials*, vol. 12, no. 9. MDPI AG, p. 1412, Apr. 30, 2019. doi: 10.3390/ma12091412.
 28. M. Babaei, M. H. Hajmohammad, and K. Asemi, “Natural frequency and dynamic analyses of functionally graded saturated porous annular sector plate and cylindrical panel based on 3D elasticity,” *Aerospace Science and Technology*, vol. 96. Elsevier BV, p. 105524, Jan. 2020. doi: 10.1016/j.ast.2019.105524.
 29. M. Babaei, F. Kiarasi, S. M. Hossaeini Marashi, M. Ebadati, F. Masoumi, and K. Asemi, “Stress wave propagation and natural frequency analysis of functionally graded graphene platelet-reinforced porous joined conical cylindrical–conical shell,” *Waves in Random and Complex Media*. Informa UK Limited, pp. 1–33, Dec. 22, 2021. doi: 10.1080/17455030.2021.2003478.
 30. F. Kiarasi, M. Babaei, K. Asemi, R. Dimitri, and F. Tornabene, “Three-Dimensional Buckling Analysis of Functionally Graded Saturated Porous Rectangular Plates under Combined Loading Conditions,” *Applied Sciences*, vol. 11, no. 21. MDPI AG, p. 10434, Nov. 06, 2021. doi: 10.3390/app112110434.
 31. F. Kiarasi, M. Babaei, S. Mollaei, M. Mohammadi, and K. Asemi, “Free vibration analysis of FG porous joined truncated conical-cylindrical shell reinforced by graphene platelets,” *Advances in nano research*, vol. 11, no. 4, pp. 361–380, Oct. 2021, doi: 10.12989/ANR.2021.11.4.361.

32. P. V. Vinh, "Analysis of bi-directional functionally graded sandwich plates via higher-order shear deformation theory and finite element method," *Journal of Sandwich Structures & Materials*, vol. 24, no. 2. SAGE Publications, pp. 860–899, Jul. 06, 2021. [doi: 10.1177/10996362211025811](https://doi.org/10.1177/10996362211025811).
33. D. H. Doan, T. Van Do, N. X. Nguyen, P. Van Vinh, and N. T. Trung, "Multi-phase-field modelling of the elastic and buckling behaviour of laminates with ply cracks," *Applied Mathematical Modelling*, vol. 94. Elsevier BV, pp. 68–86, Jun. 2021. [doi: 10.1016/j.apm.2020.12.038](https://doi.org/10.1016/j.apm.2020.12.038).
34. L. Hadji, A. Fallah, and M. M. Aghdam, "Influence of the distribution pattern of porosity on the free vibration of functionally graded plates," *Structural Engineering and Mechanics*, vol. 82, no. 2, pp. 151–161, Apr. 2022, [doi: 10.12989/SEM.2022.82.2.151](https://doi.org/10.12989/SEM.2022.82.2.151).
35. H. M. Lu, W. Zhang, and J. J. Mao, "Buckling Analyses of Functionally Graded Graphene Nanoplatelets Reinforced Nonlocal Piezoelectric Microplate," *IOP Conference Series: Materials Science and Engineering*, vol. 774, no. 1. IOP Publishing, p. 012103, Mar. 01, 2020. [doi: 10.1088/1757-899x/774/1/012103](https://doi.org/10.1088/1757-899x/774/1/012103).
36. L. Czechowski, Z. Kołakowski, Analysis of the Functionally Step-Variable Graded Plate Under In-Plane Compression, *Materials* 12/24 (2019). [DOI: 10.3390/ma12244090](https://doi.org/10.3390/ma12244090)
37. E. K. Njim, S. H. Bakhy, and M. Al-Waily, "Analytical and Numerical Investigation of Free Vibration Behavior for Sandwich Plate with Functionally Graded Porous Metal Core," *Pertanika Journal of Science and Technology*, vol. 29, no. 3. Universiti Putra Malaysia, Jul. 31, 2021. [doi: 10.47836/pjst.29.3.39](https://doi.org/10.47836/pjst.29.3.39).
38. ASTM D638, standard test method for tensile properties of plastics, *Annual Book of ASTM Standards*, American Society of Testing and Materials, West Conshohocken, 2014.
39. ASTM E 8M–00b, Standard Test Methods for Tension Testing of Metallic Materials [Metric], An American National Standard 2, 2001.
40. ASTM E1251-94, Standard Test Method for Optical Emission Spectrometric Analysis of Aluminum and Aluminum Alloys by the Argon Atmosphere, Point-to-Plane, Unipolar Self-Initiating Capacitor Discharge, ASTM International, 1999.
41. E. K. Njim, S. H. Bakhy, and M. Al-Waily, "Optimisation Design of Functionally Graded Sandwich Plate with Porous Metal Core for Buckling Characterisations," *Pertanika Journal of Science and Technology*, vol. 29, no. 4. Universiti Putra Malaysia, Oct. 29, 2021. [doi: 10.47836/pjst.29.4.47](https://doi.org/10.47836/pjst.29.4.47).
42. E. K. Njim, "Analytical and numerical flexural properties of polymeric porous functionally graded (PFGM) sandwich beams," *Journal of Achievements in Materials and Manufacturing Engineering*, vol. 110, no. 1. Index Copernicus, pp. 5–10, Jan. 01, 2022. [doi: 10.5604/01.3001.0015.7026](https://doi.org/10.5604/01.3001.0015.7026).
43. Njim, E. K., Sadiq, S. E., Tahir, M. S. A.-D., Flayyih, M. A., & Hadji, L. (2023). Flexural Bending and Fatigue Analysis of Functionally Graded Viscoelastic Materials: Experimental and Numerical Approaches. In *Physics and Chemistry of Solid State* (Vol. 24, Issue 4, pp. 628–639). Vasyl Stefanyk Precarpathian National University. <https://doi.org/10.15330/pcss.24.4.628-639>
44. Jweeg, M. J., Njim, E. K., Abdullah, O. S., Al-Shammari, M. A., Al-Waily, M., & Bakhy, S. H. (2023). Free Vibration Analysis of Composite Cylindrical Shell Reinforced with Silicon Nano-Particles: Analytical and FEM Approach. In *Physics and Chemistry of Solid State* (Vol. 24, Issue 1, pp. 26–33). Vasyl Stefanyk Precarpathian National University. <https://doi.org/10.15330/pcss.24.1.26-33>
45. K.-F. Arndt and M. D. Lechner, Eds., *Polymer Solids and Polymer Melts—Mechanical and Thermomechanical Properties of Polymers*. Springer Berlin Heidelberg, 2014. [doi: 10.1007/978-3-642-55166-6](https://doi.org/10.1007/978-3-642-55166-6).